Pilots Optimization and Surface Area Effects on Channel Estimation in RIS Aided MIMO System

Muhammad HAROON AURANGZEB, Faisal AKRAM, Imran RASHID, Attiq AHMED

Dept. of Electrical Engineering, College of Signals, National University of Science and Technology (NUST), Pakistan

haroonkhattak@mcs.edu.pk, faisal.akram@mcs.edu.pk, irashid@mcs.edu.pk, attiq@mcs.edu.pk

Submitted August 8, 2022 / Accepted March 10, 2023 / Online first March 24, 2023

Abstract. *Reconfigurable intelligent surface (RIS) is an emerging tool for 5G and wireless communication technologies that have attracted researchers' interest. However, the passive nature and the high number of reflecting elements in RIS result in a large pilot overhead, which makes channel estimation challenging in multi-user multiple-input multiple-output (MU-MIMO) wireless communication systems. Previous works have shown an improvement in reducing the pilot overhead by exploiting the structured sparsity in rows and columns, which was further improved by compensating offset among users in angular cascaded channels of RIS aided system. To further reduce the pilot overhead, we analyze and adopt coherence-optimized pilots for channel estimation and propose an algorithm to analyze the combined effect of low-coherence pilots with an optimum size of RIS elements for a given number of users, transmit antennas, and normalized error threshold performance. The simulation results illustrate better NMSE performance as compared to contemporary techniques.*

Keywords

Channel estimation, compressed sensing, reconfigurable intelligent surface, mm-wave MIMO communication, sparse channel

1. Introduction

According to CISCO estimate, there will be 29.3 billion networked devices by 2023 and the number of mobile subscribers will rise to 5.7 billion (71 percent of the population) globally [1]. By the year 2026, the overall mobile data usage will increase to 220 million terabytes per month [2]. With the introduction of 5G, a new vision of mobile communications has emerged with three distinct use cases: machine-type communications, ultra-reliable and low-latency connections, and improved broadband mobile communication. During the standardization of the 5G wireless network, no single enabling technology can satisfy all the requirements of 5G applications. Researchers have already begun to investigate communication technologies even the 6^{th} generation (6G) by moving away from the comfort zone of 5G-focused solutions.

RIS has given a new paradigm to wireless communication, especially in 5G and beyond [3–5]. The RIS technology has piqued the interest of the wireless community by regulating the electromagnetic reaction of the surrounding objects and by controlling the propagation environment deterministically, which results in improved signal quality [3]. The RIS system consists of several passive reflecting devices that may individually alter the amplitude, phase, and polarization of the incident signal. When compared to traditional active antenna arrays, the RIS reflecting devices passively reflect the impinging signals, hence no radio frequency (RF) chains are needed for transmission. As a result, it can be used with less hardware/energy cost. Its purpose is to aid transmission between transmitter and receiver by intelligently structuring wireless situations where line-of-sight (LOS) is not available.

The RIS's components are passive and unable to broadcast, receive, or process pilot signals, which makes the acquisition of channel state information (CSI) challenging. The transmission design requires the CSI of the cascaded base station (BS)-RIS-user channel, a byproduct of the BS-RIS and-user channel. Resultantly, most of the contributors focused on cascaded channel estimation [6–13]. The least square (LS) technique was proposed in [6], however, it has a high pilot overhead and grows with the number of RIS elements. To decrease the pilot cost, [7] created a transmission protocol that executes channel estimation and phase shift optimization sequentially with a pilot overhead of subgroups and divided the RIS into smaller groups. The authors of [8] presented a channel estimation approach in which the number of antennae has an inverse relationship with pilot overhead at the BS. In a rich scattering communication environment, the estimation approach in [8] requires a minimal amount of pilot overhead with a full rank cascaded channel, however, it is not suitable in millimeter-wave communications (mm wave) because the channel matrix is rank deficient. To solve this issue, the authors of [9–12] proposed compressed sensing (CS) algorithms for channel estimation with lower pilot overhead in mm-wave communication systems. The author of [9] created a sparse signal recovery issue for cascaded

DOI: 10.13164/re.2023.0187

channel estimation without taking into account the common properties of the cascaded channel in SU-MISO systems, which results in high estimation error and power leakage. The atomic norm minimization approach was used in [10] to estimate the sparse angles and gains to lessen the impact of power leakage. For the multi-user MIMO system, double structured sparsity and shared parameters were examined by both [11] and [12] to estimate multi-user cascaded channels with less pilot overhead and good estimation accuracy. Multi-user triple structured compressive sensing (MTSCS) technique was proposed in [13] for the mm-wave system by exploiting the sparse structure and iteratively optimizing the offset and beam angles to reduce the pilot overhead.

Qingqing et al. in [14], signal propagation and reflections between transmitters and receivers are intelligently coordinated by RIS. The desired realizations are achieved by efficiently mitigating the fading impairment and interference, thus improving the wireless communication capacity and reliability. Real-time reconfigurable scattering features such as delay, amplitude, and polarization are available in RIS that may be changed to increase the communication performance [15]. The RIS consists of N numbers of elements as two-dimensional surface arrays with a programmable time delay that can re-radiate without amplifying signals and if the time delay is set properly, it can contribute positively to the receiver [16]. Since RIS has reconfigurable properties and large arrays [17], the key benefit of large arrays is that signal-to-noise ratio (SNR) increases with the number of elements N [18]. Passive beam formation is achievable when meta-surfaces re-radiate a signal proportional to the surface area. When RIS re-transmits the signal, the time-delay and array gain in N numbers of the elements results in SNR at the receiver which is proportionate to N^2 and referred as "square law" [16], [19]. In [17], RIS is considered as a surface having real-time adjustable scattering qualities which add controllable paths at the physical layer and can be utilized to improve the overall performance of communication. However, large number of RIS elements makes the channel dimension much larger and results in a sharp increase in the pilot overhead of channel estimation. To reduce the pilot overhead we proposed a sparse RIS in [20] by randomly selecting elements from the RIS structure using a Gaussian distribution in the uniform planar array (UPA). To the best of our knowledge, to reduce the pilot overhead in RIS-aided system, the pilot optimization technique has not yet been studied. In this contribution, we will analyze the effect of coherent training pilots using an optimization algorithm. We will also study the effects of various surface areas of RIS to reduce pilot overhead. Based on the preceding discussion, the main contributions of this work are as follows:

- Compressed sensing (CS) allows reliable reconstruction of sparse signals. Reconstruction efficiency further improves by minimizing the mutual coherence of the measurement matrix. In this contribution, coherence optimized pilots are used to minimize the pilot overhead for channel estimation in RIS assisted systems.
- To analyze the combined effects of low coherence pilots with optimal RIS elements, an optimization algorithm is proposed. The proposed algorithm determines the optimal size of RIS's surface area and pilots.
- We show numerically that the proposed cascaded channel estimation strategy outperforms the existing double-structured orthogonal matching pursuit (OMP)-based channel estimation algorithm and the multi-user triple-structured compressive sensing simultaneous orthogonal matching pursuit algorithm in terms of normalized mean squared error (NMSE) and pilot overhead. Furthermore, the suggested estimation algorithm's NMSE performance is close to the lower bound at low SNR.

The remaining portions of the paper are structured as follows: in Sec. 2, we introduced the system model; in Sec. 3, we compared the coherence of random pilots with proposed pilots; and in Sec. 4, simulation results are compared with proposed coherence pilots technique to demonstrate the improved system performance.

2. System Model

In this section, the cascaded channel in RIS aided wireless system is introduced in the first part and in the second part, the channel estimation problem is formulated. The cascaded channels are sparse in nature by exploiting the sparsity, CS-based approaches are used in channel estimation. Accurate channel models are needed for RIS-assisted communication to be effective. In a RIS-assisted situation, we will use cascaded channel estimation and develop a channel estimation problem.

2.1 Cascaded Channel

In this study, the widely used Saleh-Valenzuela channel model is adopted [21]. We assume a narrowband mm-wave MIMO wireless system with i single antenna users connecting with a BS in an uplink system, where the BS has $N_{\mathrm{T_x}} \times N_{\mathrm{T_y}}$ transmit antennas and $N_{\mathrm{R_x}} \times N_{\mathrm{R_y}}$ receive antennas at RIS having uniform planar arrays (UPA) antenna which serves i users simultaneously. Let $\mathbf{H}_{\mathrm{G}}$, serves as channel between BS and RIS and $\mathbf{H}_{\mathrm{r},i}$ can be defined as channel between RIS and i^{th} user, where $(i = 1, 2, \ldots I)$. The channel $\mathbf{H}_{\mathrm{G}}$ can be represented as

$$\mathbf{H}_{\mathrm{G}} = \sqrt{\frac{N_{\mathrm{T}} N_{\mathrm{R}}}{P_{\mathrm{G}}}} \sum_{\ell_1=1}^{P_{\mathrm{G}}} \alpha_{\ell_1}^{\mathrm{G}} \mathbf{a}_{\mathrm{R}}(\theta_{\ell_1}^{\mathrm{r}}, \omega_{\ell_1}^{\mathrm{r}}) \mathbf{a}_{\mathrm{T}}^{\mathrm{H}}(\theta_{\ell_1}^{\mathrm{t}}, \omega_{\ell_1}^{\mathrm{t}}) \quad (1)$$

where P_{G} are the l^{th} paths among BS and RIS, $\alpha_{\ell}^{\mathrm{G}}$ represent the complex gain, whereas $\theta_{\ell_1}^{\mathrm{t}}, \omega_{\ell_1}^{\mathrm{t}}$ represent the azimuth and elevation angles at BS and at RIS it is represented by $\theta_{\ell_1}^{\mathrm{r}}, \omega_{\ell_1}^{\mathrm{r}}$. The corresponding array steering vectors of BS and RIS are $\mathbf{a}_{\mathrm{T}} \in \mathbb{C}^{N_{\mathrm{T}} \times 1}$ and, $\mathbf{a}_{\mathrm{R}} \in \mathbb{C}^{N_{\mathrm{R}} \times 1}$ respectively. Let the size of channel $\mathbf{H}_{\mathrm{G}}$ be $N_{\mathrm{T}} \times N_{\mathrm{R}}$, where N_{T} is defined as $N_{\mathrm{T_x}} \times N_{\mathrm{T_y}}$ and N_{R} as $N_{\mathrm{R_x}} \times N_{\mathrm{R_y}}$. The following may be used to illustrate the channel between RIS and i^{th} user:

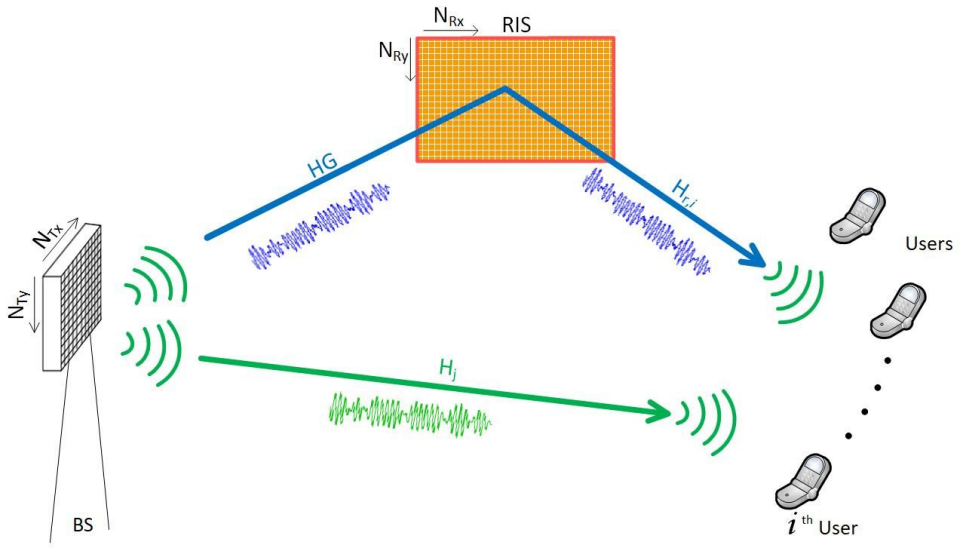

Fig. 1. RIS system model.

$$\mathbf{H}_{\mathrm{r},i} = \sqrt{\frac{N_{\mathrm{R}}}{P_{\mathrm{r},i}}} \sum_{\ell_2=2}^{P_{\mathrm{r},i}} \alpha_{\ell_2}^{\mathrm{r},i} \mathbf{a}_{\mathrm{T}} \left(\theta_{\ell_2}^{\mathrm{r},i} \omega_{\ell_2}^{\mathrm{r},i}\right) \tag{2}$$

where $\theta^{\mathrm{r},i}$, $\omega^{\mathrm{r},i}$ are the azimuth and elevation angles at RIS, $\alpha_{\ell_2}^{\mathrm{r},i}$ defines the complex gain and $P_{\mathrm{r},i}$ denote the paths between RIS and i^{th} user. The angular antenna response in uniform planar array is denoted by

$$\mathbf{a}_{\mathrm{UPA}}(\theta,\omega) = \sqrt{\frac{1}{N_{\mathrm{R_y}}}} \left[\mathrm{e}^{-\mathrm{j}2\pi d \sin(\omega)\cos(\theta) n_1/\lambda}\right] \otimes \tag{3}$$

$$\left[\mathrm{e}^{-\mathrm{j}2\pi d \sin(\phi) n_2/\lambda}\right] \tag{4}$$

where $\otimes$ represents the Kronecker product of two angular arrays. $\mathbf{n}_1 = [1,\ldots,N_{\mathrm{R_x}}]$ and $\mathbf{n}_2 = [1,\ldots,N_{\mathrm{R_y}}]$ denotes the components for each channel. The i^{th} user's cascaded channel can be represented by $\mathbf{H}_{\mathrm{RIS}} \triangleq \mathbf{H}_{\mathrm{G}}\mathrm{diag}(\mathbf{H}_{\mathrm{r},i})$, where $\mathbf{H}_{\mathrm{RIS}} \in \mathbb{C}^{N_{\mathrm{T}} \times N_{\mathrm{R}}}$, can be decomposed as

$$\mathbf{H}_{\mathrm{RIS}} = \mathbf{A}_{N_{\mathrm{T}}} \tilde{\mathbf{H}}_{\mathrm{RIS}} \mathbf{A}_{N_{\mathrm{R}}}^{\mathrm{T}} \tag{5}$$

where $\hat{\mathbf{H}}_{\mathrm{RIS}}$ denote the angular cascaded channel. $\mathbf{A}_{N_{\mathrm{T}}}$ and $\mathbf{A}_{N_{\mathrm{R}}}$ are unitary dictionary matrices of size $N_{\mathrm{T}} \times N_{\mathrm{T}}$ and $N_{\mathrm{R}} \times N_{\mathrm{R}}$ at BS and RIS respectively. The cascaded channel is sparse and has few nonzero elements because of limited scattering around BS and RIS [12].

2.2 Problem Formulation

In a traditional wireless system, the channel is known to the base station (BS) and can easily be estimated, on the other hand, channel estimation in RIS aided system is a difficult task as pilot overhead is large because of more number of RIS elements. The UPA cascaded channel is represented as:

$$\tilde{\mathbf{H}}_{\mathrm{RIS}} = \sqrt{\frac{N_{\mathrm{T}} N_{\mathrm{R}}}{P_{\mathrm{G}} P_{\mathrm{r},i}}} \sum_{\ell_1=1}^{P_{\mathrm{G}}} \sum_{\ell_2=2}^{P_{\mathrm{r},i}} \alpha_{\ell_1}^{\mathrm{G}} \alpha_{\ell_2}^{\mathrm{r},i} \hat{\mathbf{a}}_{\mathrm{R}}(\theta_\gamma^{\mathrm{r}}, \omega_\gamma^{\mathrm{r}}) \hat{\mathbf{a}}_{\mathrm{T}}^{\mathrm{H}}(\theta_\gamma^{\mathrm{t}}, \omega_\gamma^{\mathrm{t}}) \tag{6}$$

where $\hat{\mathbf{a}}_{\mathrm{R}}(\theta_\ell^{\mathrm{r}}, \omega_\gamma^{\mathrm{r}}) = \mathbf{A}_{N_{\mathrm{T}}}^{\mathrm{H}} \mathbf{a}_{\mathrm{R}}(\theta_\ell^{\mathrm{r}}, \omega_\ell^{\mathrm{r}})$ and $\hat{\mathbf{a}}_{\mathrm{T}}(\theta_\ell^{\mathrm{r}}, \omega_\ell^{\mathrm{r}}) = \mathbf{A}_{N_{\mathrm{R}}}^{\mathrm{H}} \mathbf{a}_{\mathrm{T}}(\theta_\ell^{\mathrm{r}}, \omega_\ell^{\mathrm{r}})$ are the only non-zero elements which are located on the array steering vector. In the RIS arrangement, the channel estimation is imprecise. To improve the channel estimation a double structured sparsity solution was proposed in [12] and similar technique is adopted in this study. The uplink channel model is considered as all users transmit known pilots to BS via RIS in Q time slots. The time slot q is defined as $(\mathbf{q} = 1, 2, \ldots, Q)$. Let $\mathbf{y}_i^{\mathrm{UL}} \in \mathbb{C}^{N_{\mathrm{T}} \times 1}$ denote the received signal and expressed as

$$\mathbf{y}_i^{\mathrm{UL}} = \mathbf{H}_{\mathrm{G}}\mathrm{diag}(\mathbf{H}_{\mathrm{r},i})\ \theta_q \Omega + \mathbf{v}_i \tag{7}$$

where $\mathbf{\Omega}$ are the pilot signals delivered to BS by i^{th} user and θ_q is the reflecting coefficient at n^{th} RIS element in q^{th} time slot. The diagonal channel matrix is denoted by $\mathrm{diag}(\mathbf{H}_{\mathrm{r},i})$ which has channel vectors on its diagonals. We can write (6) as

$$\mathbf{y}_i^{\mathrm{UL}} = \mathbf{H}_{\mathrm{RIS}}\ \theta_q \Omega + \mathbf{v}_i, \tag{8}$$

let assume $\mathbf{\Omega} = 1$ and after Q time slot transmission $\mathbf{Y}_i$=$[y_{i,1} \ldots Y_{i,Q}]$ is obtained

$$\mathbf{Y}_i = \mathbf{H}_{\mathrm{RIS}} \mathbf{\Theta} + \mathbf{v}_i \tag{9}$$

where $\mathbf{\Theta} = [\theta_1, \ldots \theta_q]$ and noise $\mathbf{v}_i = [v_{i,1} \ldots v_{i,Q}]$ from (4) and (7) we get

$$\mathbf{Y}_i = \mathbf{\Theta} \mathbf{A}_{N_{\mathrm{T}}} \tilde{\mathbf{H}}_{\mathrm{RIS}} \mathbf{A}_{N_{\mathrm{R}}}^{\mathrm{T}} + \mathbf{v}_i. \tag{10}$$

Let $\tilde{\mathbf{Y}}_i = (\mathbf{A}_{N_{\mathrm{T}}}^{\mathrm{H}} \mathbf{Y}_i)^{\mathrm{H}}$ is the effective measurement matrix of size $Q \times N_{\mathrm{T}}$ and $\hat{\mathbf{v}}_i = (\mathbf{A}_{N_{\mathrm{T}}}^{\mathrm{H}} \mathbf{v}_i)^{\mathrm{H}}$ as noise matrix of size $Q \times N_{\mathrm{T}}$. We can write (9) as

$$\tilde{\mathbf{Y}}_{\mathbf{i}} = \tilde{\mathbf{\Theta}} \tilde{\mathbf{H}}_{\mathrm{RIS}}^{\mathrm{H}} + \tilde{\mathbf{v}}_i \tag{11}$$

where $\tilde{\mathbf{\Theta}} = (\mathbf{A}_{N_R}^{T} \mathbf{\Theta})^{H}$ is sensing matrix of size $Q \times N_R$ [12], the cascaded channel can be estimated using CS algorithms. As compared to a traditional wireless system, the RIS-aided system have a large array of elements resulting in large channel dimensions and pilot overhead. Furthermore, due to a lack of RF chains, acquiring the CSI is difficult [22].

3. CS Base Channel Estimation

In traditional digital signal processing, the Nyquist criteria state that a band-limited signal must have a sampling frequency at least twice its bandwidth to obtain precise signal reconstruction. On the other hand, in CS framework, the signal can be recovered even when the number of accessible samples is significantly less than the conventional requirements [23], [24]. CS addresses the accurate recovery of unknown sparse signals from under-determined linear measurements [23–26]. It demonstrates how to recover a sparse signal from a reduced number of incoherent samples. Consider $\mathbf{x} \in \mathbb{C}^N$ is sparse vector, $\mathbf{\Phi} \in \mathbb{C}^{M \times N}$ is the measurement matrix and $\mathbf{y} \in \mathbb{C}^M$ is the measurement vector, where $\mathbf{y} = \mathbf{\Phi x}$ and $M < N$. In the case of sparse $\mathbf{x}$, the following minimization can be used to minimize the issue:

$$\min \|\mathbf{x}\|_0 \quad \text{s.t} \quad \mathbf{y} = \mathbf{\Phi x}.$$

There are two main principles that need to be considered when using CS framework for channel estimation. These principles ensure that CS is effective and solves the reconstruction problems. The first principle is sparsity and the second is mutual coherence. A signal $x \in \mathbb{C}^N$ is said to be sparse if it has $k << N$ number of non-zero elements. A sparse signal can be efficiently compressed by keeping only its nonzero coefficients' position and values [25]. In contrast to the Nyquist theorem's requirements, compressed sensing allows efficient data sampling at significantly lower rates.

The second important property which ensures the reconstruction is mutual coherence. The coherence of a square matrix is always orthogonal whereas, in a rectangular matrix, orthogonality is not possible. Matrix $\mathbf{A}$ with low coherence is known to have better recovery of sparse signal. The coherence of matrix $\mathbf{A}$ can be defined as:

$$\mu(\mathbf{A}) = \max_{i \neq j} \frac{|\langle a_i, a_j \rangle|}{\|a_i\| \, \|a_j\|} \tag{12}$$

where $\mu(A)$ is the largest absolute inner product between column a_i and a_j [25].

In RIS systems, channel estimation is challenging as compared to traditional wireless communication, mainly due to two reasons. First, RIS elements are passive in nature, second, more elements at RIS make the channel dimension much larger which sharply increases the pilot overhead. In [22], sparsity based channel estimation was proposed to lower the pilot overhead. Conventional wireless systems have limited propagation paths between the user and BS, which results in a sparse channel between the user and BS in the angular domain. Similarly, in RIS system, the cascaded channel

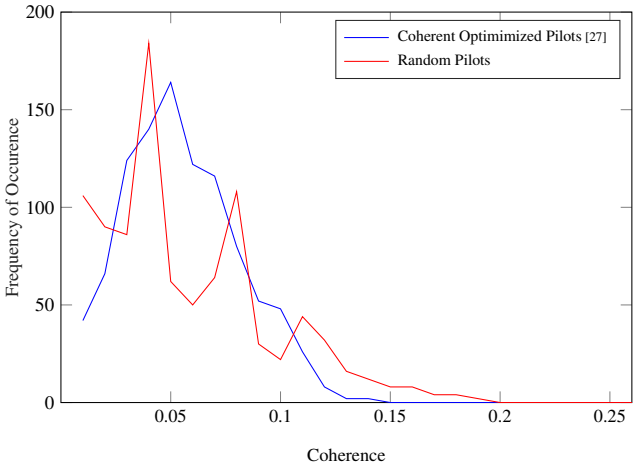

Fig. 2. Coherent vs random matrix coherence comparison.

$\mathbf{H}_{RIS} \in \mathbb{C}^{N_T \times N_R}$ is also sparse in the angular domain. The channel can be decomposed as in (4). Xiuhong et al. in [12] exploited the DS sparsity of the angular cascaded channel and proposed a DS-OMP algorithm for channel estimation, which results in low pilot overhead. A similar recovery algorithm is adopted in this contribution. As discussed above, the performance of CS also depends on the coherence of the sensing matrix. In [12], pilot overhead was reduced by exploiting the sparsity, however, random pilots were adopted. In order to further reduce the pilot overhead in RIS assisted system, the coherence of sensing matrix is optimized by using the proposed optimization algorithm of [27]. Figure 2 illustrates the comparison of coherence optimization of the random matrix with coherence optimized matrix, using optimization algorithm [27].

4. Proposed Algorithm for Pilot Optimization

This section proposes an algorithm to determine the optimum size of RIS as well as the optimum pilot overhead in a given environment. In the proposed algorithm, the optimum size of RIS is obtained by setting a threshold of bit error after successive iterations. Different rectangular shaped RISs' are analyzed to get the optimum RIS size. The reduced size of RIS results in a lesser number of arrays, thus minimizing the pilot overhead while achieving acceptable NMSE performance.

The main procedure of the proposed algorithm can be explained as follows. The channel matrix, sensing matrix, bit error threshold, and RIS elements are initialized in steps 1–4. Because of row structured sparsity, the common row support is determined jointly, and then common column support is calculated by exploiting partial column-structured sparsity. Finally, each user-specific column support for i user is evaluated separately, and then the channel is estimated in steps 6–10 [12]. In step 11, the spatial domain cascaded channel is obtained. Average NMSE is calculated by taking

the norm of the difference between the original and estimated channel in step 12. To obtain optimized RIS, an error threshold value η is selected. The difference between average NMSE and η is returned to Γ in step 14. When the difference of average NMSE and η becomes zero or less than zero, the optimum size of RIS is obtained for optimum NMSE threshold error in steps 15–23.

Algorithm 1: Optimize RIS for given environment

input : $\mathbf{Y}_{k_{Q\times N_T}}, \mathbf{\Theta}_{Q\times N_R}, \mathbf{A}_{N_T} \in \mathbb{C}^{N_T\times N_T}, \mathbf{A}_{N_R} \in \mathbb{C}^{N_R\times N_R}, I, Q, P_G$

Initialize: $\mathbf{H}_{RIS} = 0_{N_T\times N_R}$; /* Channel Matrix */

1 $\tilde{\mathbf{\Theta}} = (\mathbf{A}^{T}_{N_R}\mathbf{\Theta})^{H}_{Q\times N_R}$; /* Sensing Matrix */

2 $\eta = 0.05$; /* Error Threshold */

3 $N_{R_x} = 2, N_{R_y} = 5$; /* Rows & Columns of RIS */

4 $N_R = N_{R_x} \times N_{R_y}$; /* Elements of RIS */

5 *Channel estimation by exploiting row and column sparsity*;

6 **for** $l_1 = 1, 2, 3, \ldots, P_G$ **do**

7 **for** $i = 1, 2, 3, \ldots, I$ **do**

8 $\tilde{\mathbf{H}}_{RIS}(\Omega_c^{l_1}, \Omega_r) = \mathbf{\Theta}^{T}(:, (\Omega_c^{l_1,i}))\mathbf{Y}_i(\Omega_r)(l_1))$; /* Channel Estimation common row & column support [12] */

9 **end**

10 **end**

11 $\mathbf{H}_{RIS} = (\mathbf{A}^{H}_{N_T}\tilde{\mathbf{H}}_{RIS}\mathbf{A}_{N_R})$; /* Cascaded Channel */

12 $NMSE_{avg} = \|\tilde{\mathbf{H}}_{RIS} - \mathbf{H}_{RIS}\|$; /* NMSE Calculation */

13 **for** $Q_i = 1, 2, 3, \ldots 7$ **do**

14 $\Gamma \leftarrow |NMSE_{avg} - \eta|$; /* Threshold */

15 **if** $\Gamma > 0$ **then**

16 $N_{R_x} \leftarrow N_{R_x} + 2$; /* Increase Rows of RIS */

17 $N_{R_y} \leftarrow N_{R_y} + 5$; /* Increase Column of RIS */

18 **else if** $\Gamma \leq 0$ **then**

19 $N_{R_{x_0}} \leftarrow N_{R_x}$; /* Return row size */

20 $N_{R_{y_0}} \leftarrow N_{R_y}$; /* Return Column size */

21 **end**

22 **end**

23 **end**

output : $\tilde{\mathbf{\Theta}}_{Q\times N_R}$; /* Sensing matrix with optimized RIS size */

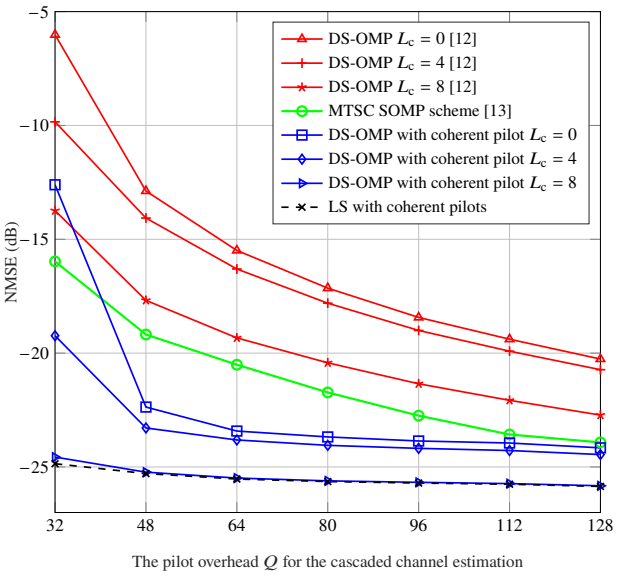

Fig. 3. Channel estimation in random pilots vs coherent pilots.

5. Simulation Results

We will compare the simulation outcomes of random pilots with coherence-optimized pilots in an uplink RIS system, and the effects of various surface areas will also be demonstrated on channel estimation in the RIS system. The effects of varied paths will also be analyzed. We consider the BS and RIS elements as $N_{T_x} = 8$, $N_{T_y} = 8$ and $N_{R_x} = 16$, $N_{R_y} = 16$ respectively, the number of users that is $I = 16$ and paths connecting RIS and BS is $P_G = 5$. The paths between RIS and i^{th} user is $P_{r,i} = 8 \ \ \forall i$. The random pilots' sensing matrix Θ selects random values from range $\{-\frac{1}{N_R}, +\frac{1}{N_R}\}$. The RIS and BS distance is denoted by $d_{BRIS} = 10$ m and the distance between RIS and i^{th} user is $d_{r,i} = 100$ m. Varied paths between RIS and i^{th} user are denoted by L_c. MATLAB R2017a is used to implement the simulations, and the system has an Intel Core i7-8565 CPU @ 4.6 GHz Quad-core 64-bit processor with 16 GB RAM.

We will compare three different scenarios to analyze channel estimation in RIS assisted system. In the first part, random pilots are compared with coherence optimized pilots and the results are illustrated. In the second part, the effects of different rectangular surface areas on channel estimation are analyzed to achieve better NMSE results and in the third part, the effect of different varied paths between the user and RIS are analyzed and illustrated.

5.1 Coherence Optimized Pilot vs Pseudo Random Pilots

Usually pseudo-random matrix is considered in mm-wave MIMO communication. We compare the randomly generated pilot matrix with a coherence optimized matrix for channel estimation in DS-OMP recovery algorithms [12] as well as in MTSC-SOMP scheme [13]. We consider LS with known coherent pilots and known channels as a theoretical benchmark. Figure 3 shows the normalized mean square error (NMSE) performance versus pilots' overhead in different time slots Q. The optimized coherence matrix results are better than contemporary techniques as illustrated in Fig. 3. Three different paths between BS and RIS are considered. When path is set as $L_c = 0$ at time slot $Q = 32$, the NMSE gap is 6 dB and at time slot $Q = 48$ the gap is increased to 9 dB. The NMSE performance of coherent pilots remains constant from time slot $Q = 64$ to $Q = 128$. As we increase the paths i.e $L_c = 4$ in the first two-time slots i.e, $Q = 32$ and $Q = 48$ the NMSE gap between conventional pilots and coherent pilots is 9 dB and remains constant from time slot $Q = 64$ to $Q = 128$. Similarly, when the paths are increased to $L_c = 8$ the NMSE performance of coherence pilots significantly improves. The NMSE gap between the conventional pilot and coherence pilot scheme is 12 dB in first time slot $Q = 32$ and in second time slot $Q = 48$, is 9 dB. The results illustrate that in the proposed scheme, with the increase in pilot length Q, the NMSE performance increases significantly in the first two slots and remains constant for other time slots and it outperforms the baseline systems while achieving similar performance to the LS coherent scheme.

5.2 Varying Surface Area

In [12], a square shape RIS was considered where elements of RIS and BS were set as $N_{R_x} = N_{R_y} = 16$ and $N_{T_x} = N_{T_y} = 8$ respectively in a cascaded channel environment. Since RIS may simulate the dispersion of arbitrary shaped objects [16], here we will analyze the different rectangular shapes of RIS and its effects on channel estimation. The findings will be examined using both traditional CS and DS-OMP techniques. We consider a rectangular surface RIS, where elements of RIS are $N_{R_x} = 24$ and $N_{R_y} = 8$ and BS elements are $N_{T_x} = N_{T_y} = 8$. The influence of reduced size RIS is visible in the double structured sparsity recovery scheme [12], and an improvement of 1.5 dB in NMSE performance is achieved, as shown in Fig. 4. However, the improvement in conventional CS is minimal.

The NMSE performance is analyzed by altering the shape of RIS. The elements of RIS are set as $N_{R_x} = 20$ and $N_{R_y} = 8$ thus reducing the surface area and pilot overhead. Results show that conventional CS scheme has an almost negligible effect on NMSE performance due to insufficient information, however as shown in Fig. 5, a significant improvement in NMSE performance of 3 dB is achieved as compared to RIS arrangement of [12]. The NMSE performance gap of 3 dB remained constant in all time slots Q.

We further analyzed the performance of RIS by altering the elements as $N_{R_x} = 22$ and $N_{R_y} = 10$. After changing the RIS elements, minor improvement in NMSE gain in the double structured recovery algorithm is achieved over Q time slots. The conventional CS has a very negligible effect, as shown in Fig. 6.

5.3 Varied Common Paths Effects

In this section, we will analyze the effects of common paths between RIS and the users in a rectangular surface area of RIS with coherence-optimized pilots. In previous work of [12], the NMSE performance improves with increase in common paths. First, we'll look at the scenarios where RIS and the users have no common route, i.e $L_c = 0$, and the elements of RIS are set as $N_{R_x} = 20$ and $N_{R_y} = 8$. Figure 7(a) shows significant improvement in NMSE performance as compared to [12]. The combined effect of shape and optimized pilots show a 6 dB gap in conventional CS and in DS recovery algorithms. With coherent pilots, a sudden increase in NMSE is observed in the first two pilot lengths i.e $Q = 32$ and $Q = 48$, and it remained constant in the pilot length $Q = 64$ to $Q = 128$.

Figure 7 illustrates the influence of the paths between RIS and the users when the common paths are set as $L_c = 4$, $L_c = 6$, and $L_c = 8$. The NMSE performance is improved and pilot overheads are further reduced as compared to contemporary techniques. When $L_c = 4$, the NMSE gain of 7 dB is seen in conventional CS and 9 dB gain in DS recovery algorithm. It further improves when $L_c = 6$, the gain of CS enhances to 8 dB and 10 dB in DS-CS.

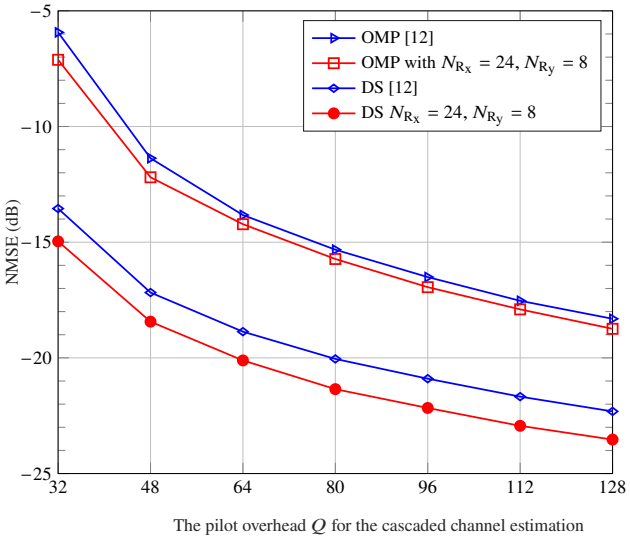

Fig. 4. Surface area variation of RIS, $N_{R_x} = 24$, $N_{R_y} = 8$.

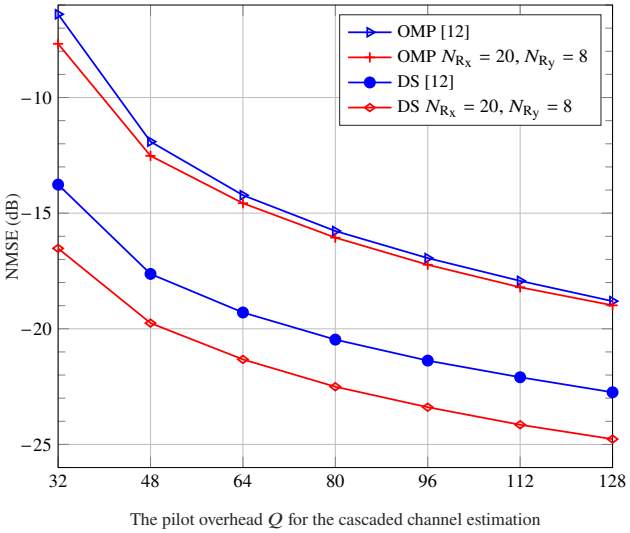

Fig. 5. Surface area variation of RIS, $N_{R_x} = 20$, $N_{R_2} = 8$.

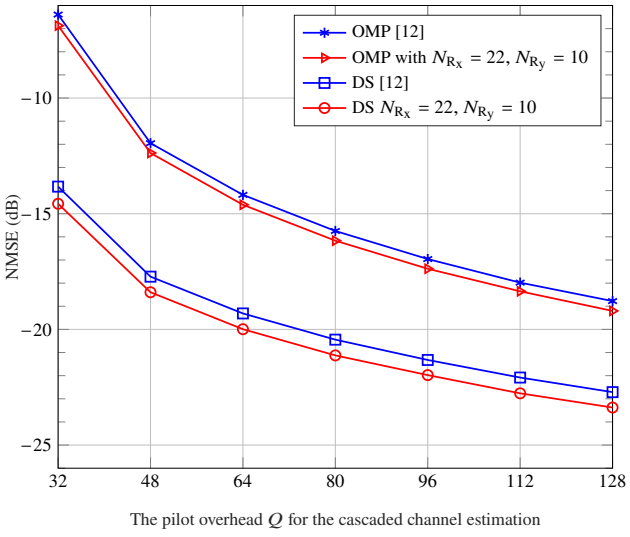

Fig. 6. Surface area variation of RIS, $N_{R_x} = 22$, $N_{R_y} = 10$.

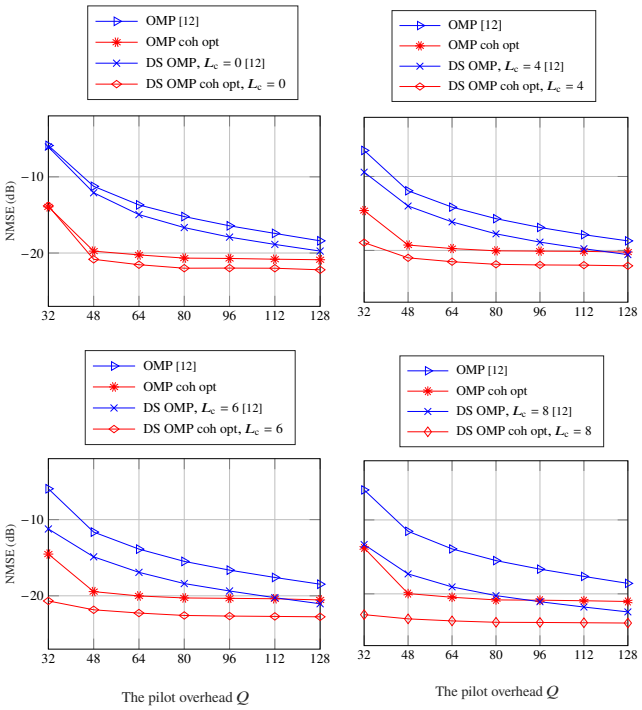

Fig. 7. Varying common path between RIS and users with reduced surface area $N_{R_x} = 20$, $N_{R_y} = 8$.

A significant improvement is seen when paths are set as $L_c = 8$ in CS and DS-CS algorithm, subsequently reducing the pilot overhead. The improvement in NMSE around 10 dB is observed in CS technique and 12 dB in DS technique. At pilot length $Q = 32$ to $Q = 48$, the conventional CS technique shows a sharp increase in NMSE which gradually improves till pilot length $Q = 128$. In DS recovery algorithm, the NMSE performance remains almost persistent from pilot length $Q = 48$ to $Q = 128$. The above results show that the burden of pilot overhead is further reduced as compared to previously proposed techniques in channel estimation by altering the shape and optimizing the training pilots.

A box plot is a graphical method of displaying the locality, spread, and skewness groups of numerical data through their quartiles. Each box has a center point that represents the median and margins, which represent the 25th and 75th percentiles of the distribution, respectively. The outliers are shown separately using the '+' sign and the whiskers are extended to the most extreme data points that are not outliers. Box plot comparison of DS-OMP with random pilots and coherence optimized pilots are shown in Fig. 8, where $L_c = 8$. Coherence optimized matrix's NMSE results show low pilot overhead and low range as compared to the random pilot, which is less consistent. The standard deviation of coherence optimized pilot also remains consistent in all time slots. The random pilots' outliers are wider than the coherence optimized pilots. The random pilot matrix NMSE plot starts from −14 dB and ends at −23 dB, whereas coherence pilot NMSE starts at −24.5 dB and ends at −25 dB for all time slots. The above analysis shows that the adopted technique has better results as compared to random pilots with reduced pilot overhead.

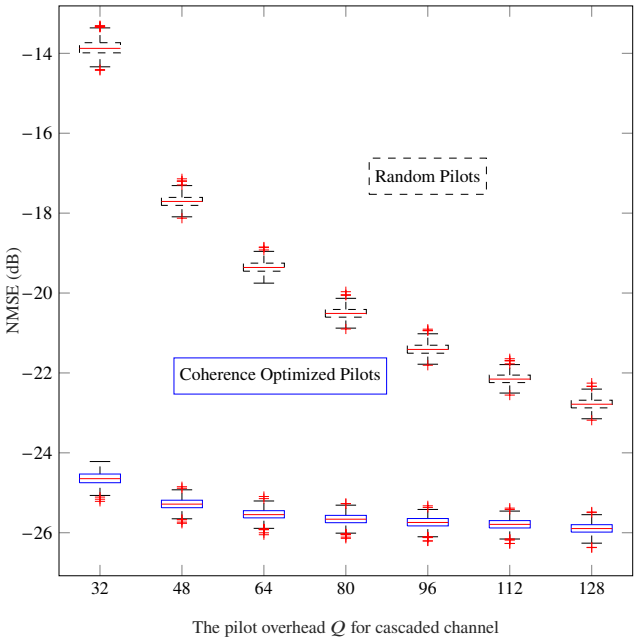

Fig. 8. Box plot DS OMP with $L_c = 8$, 500 iterations.

5.4 Real Time Implementation

To implement the simulations in real-time scenarios, the run-time and NMSE variations of coherence optimized pilot schemes were analyzed with different RIS sizes and common paths. The simulation time data with the corresponding NMSE of 100 iterations is presented with box plot and illustrated in Figs. 9 and 10. In the first case, we set elements of RIS as $N_{R_x} = 16$ and $N_{R_y} = 16$, and the run-time was analyzed with various common paths. When no common path is considered between the user and RIS i.e. $L_c = 0$ and the pilot length is set as $Q = 32$, the average simulation run-time is 19 secs and when the pilot length Q is increased from 48 to 128, the average run-time also increases from 21 secs to 28 secs as illustrated in Fig. 9(a). When the common paths are set as $L_c = 4$, the average run time at pilot length $Q = 32$ increased to 24 secs and at $Q = 128$ the average run-time increased to 36 secs as illustrated in Fig. 9(b). At $L_c = 6$ the average simulation time at $Q = 32$ is 22 secs and at Q=128 is 33 secs and when the common path is further increased to $L_c = 8$, the average run-time is 20 secs, at pilot length $Q = 32$ and at $Q = 128$ the average run-time increases to 30 secs as illustrated in Fig. 9(c) and (d). The corresponding NMSE box plots of 100 iterations are also shown in Fig. 9(e)–(h). In the next scenario, we changed the shape of RIS to rectangular, and the elements of RIS are set as $N_{R_x} = 20$ and $N_{R_y} = 10$. When $L_c = 0$ the average run-time at pilot length $Q = 32$ is reduced to 10 secs as compared to the previous RIS setting which was 19 sec. When pilot length Q is increased from 48 to 128 the average simulation time also increases to 11 sec and 15 secs respectively as illustrated in Fig. 10(a). Similarly, run-time at $L_c = 4$, $L_c = 6$ and $L_c = 8$, is illustrated in Fig. 10(b)–(d). The results show that the average run-time reduces to 45% as compared to previous RIS settings. The results show that at optimum RIS size, the average simula-

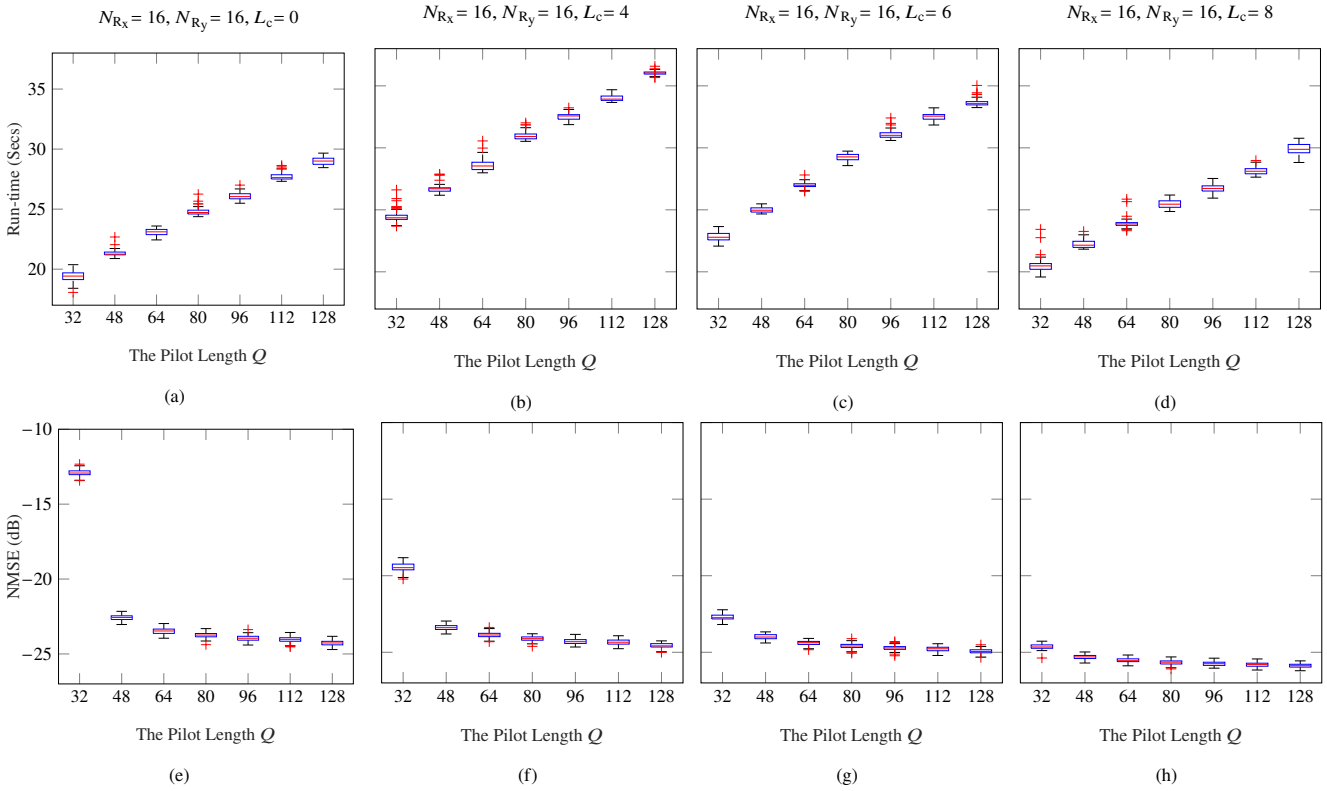

Fig. 9. Simulation run-time and NMSE with $N_{R_x} = 16$, $N_{R_y} = 16$, $N_{T_x} = 8$, $N_{T_y} = 8$, $i = 16$.

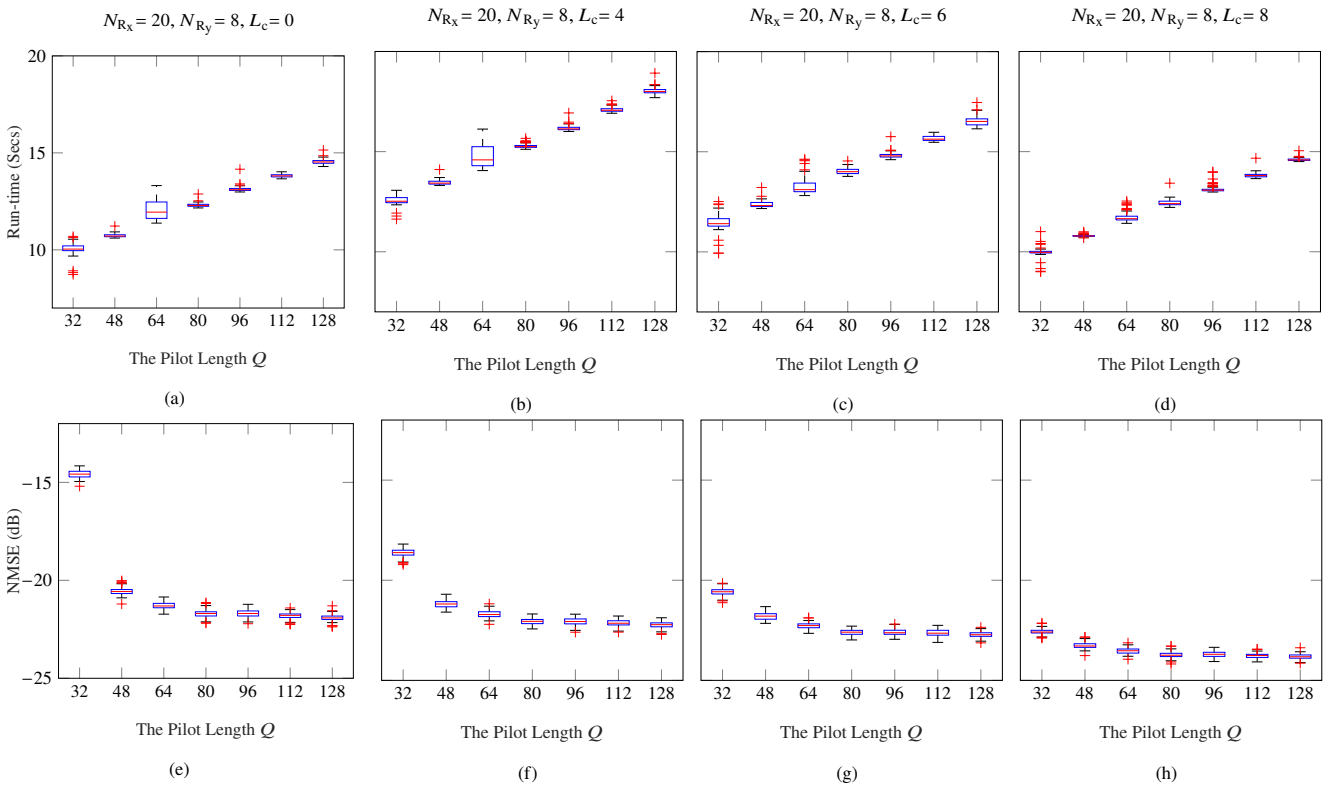

Fig. 10. Simulation run-time and NMSE with $N_{R_x} = 20$, $N_{R_y} = 8$, $N_{T_x} = 8$, $N_{T_y} = 8$, $i = 16$.

tion time also improves and variations in NMSE and run-time remain minimum. The simulations can be implemented in a real-time scenario by incorporating the already optimized matrix with different sizes of RIS, various paths, and pilot lengths at an optimum threshold value of NMSE.

6. Conclusion

In this contribution, we use the coherence optimized pilots and the influence of different surface areas in RIS assisted mm-wave multi-user MIMO system to reduce the pilot overhead and the effects of varied paths on NMSE performance. We also proposed an algorithm for the optimal size of RIS in a given environment. Simulation findings demonstrate that the selected method requires pilot overhead, which is much lower than the existing algorithms. We employ a Grassmannian sensing matrix in DS-OMP as well as in the conventional CS recovery algorithm. It was discovered that the NMSE gain in different time slots has significant improvement. According to the outcomes of the study, the coherence-optimized pilots have significant effects coupled with diverse shaped structures, which resulted in substantial improvement. In this contribution, we analyzed rectangular-shaped RIS. For future work, the effects of more arbitrary shapes like circular, elliptical, triangular, and pentagon can be analyzed and explored.

References

[1] CISCO. *Annual Internet Report (2018–2023) White Paper*. 2020, [Online]. Available at: http://www.cisco.com/c/en/us/solutions/collateral/executive-perspectives/annual-internet-report/white-paper-c11-741490.html

[2] REPORT LINKER. *Global Mobile Data Traffic Industry*. 2022, [Online]. Available at: http://www.reportlinker.com/p05442636/Global-Mobile-Data-Traffic-Industry.html

[3] BASAR, E., DI RENZO, M., DE ROSNY, J., et al. Wireless communications through reconfigurable intelligent surfaces. *IEEE Access*, 2019, vol. 7, p. 116753–116773. DOI: 10.1109/ACCESS.2019.2935192

[4] LIASKOS, C., NIE, S., TSIOLIARIDOU, A., et al. A new wireless communication paradigm through software-controlled metasurfaces. *IEEE Communications Magazine*, 2018, vol. 56, no. 9, p. 162–169. DOI: 10.1109/MCOM.2018.1700659

[5] RENZO, M. D., DEBBAH, M., PHAN-HUY, D.T., et al. Smart radio environments empowered by reconfigurable AI meta-surfaces: An idea whose time has come. *EURASIP Journal on Wireless Communications and Networking*, 2019, p. 1–20. DOI: 10.1186/s13638-019-1438-9

[6] JENSEN, T. L., DE CARVALHO, E. An optimal channel estimation scheme for intelligent reflecting surfaces based on a minimum variance unbiased estimator. In *IEEE International Conference on Acoustics, Speech and Signal Processing (ICASSP)*. Barcelona (Spain), 2020, p. 5000–5004. DOI: 10.1109/ICASSP40776.2020.9053695

[7] ZHENG, B., ZHANG, R. Intelligent reflecting surface-enhanced OFDM: Channel estimation and reflection optimization. *IEEE Wireless Communications Letters*, 2020, vol. 9, no. 4, p. 518–522. DOI: 10.1109/LWC.2019.2961357

[8] WANG, Z., LIU, L., CUI, S. Channel estimation for intelligent reflecting surface assisted multiuser communications: Framework, algorithms, and analysis. *IEEE Transactions on Wireless Communications*, 2020, vol. 19, no. 10, p. 6607–6620. DOI: 10.1109/TWC.2020.3004330

[9] WANG, P., FANG, J., DUAN, H., et al. Compressed channel estimation for intelligent reflecting surface-assisted millimeter wave systems. *IEEE Signal Processing Letters*, 2020, vol. 27, p. 905–909. DOI: 10.1109/LSP.2020.2998357

[10] HE, J., WYMEERSCH, H., JUNTTI, M. Channel estimation for RIS-aided mmwave MIMO systems via atomic norm minimization. *IEEE Transactions on Wireless Communications*, 2021, vol. 20, no. 9, p. 5786–5797. DOI: 10.1109/TWC.2021.3070064

[11] CHEN, J., LIANG, Y. C., CHENG, H. V., et al. Channel estimation for reconfigurable intelligent surface aided multi-user MIMO systems. *arXiv*:1912.03619, 2019, p. 1–16. DOI: 10.48550/arXiv.1912.03619

[12] WEI, X., SHEN, D., DAI, L. Channel estimation for RIS assisted wireless communications - Part II: An improved solution based on double structured sparsity. *IEEE Communications Letters*, 2021, vol. 25, no. 5, p. 1403–1407. DOI: 10.1109/LCOMM.2021.3052787

[13] SHI, X., WANG, J., SONG, J. Triple-structured compressive sensing-based channel estimation for RIS-aided MU-MIMO systems. *IEEE Transactions on Wireless Communications*, 2022, vol. 21, no. 12, p. 1109–11109. DOI: 10.1109/TWC.2022.3189686

[14] WU, Q., ZHANG, S., ZHENG, B., et al. Intelligent reflecting surface aided wireless communications: A tutorial. *IEEE Transactions on Communications*, 2021, vol. 69, no. 5, p. 3313–3351. DOI: 10.1109/TCOMM.2021.3051897

[15] TSILIPAKOS, O., TASOLAMPROU, A. C., PITILAKIS, A., et al. Toward intelligent metasurfaces: The progress from globally tunable metasurfaces to software-defined metasurfaces with an embedded network of controllers. *Advanced Optical Materials*, 2020, vol. 8, no. 17, p. 1–18. DOI: 10.1002/adom.202000783

[16] BJÖRNSON, E., ÖZDOGAN, Ö., LARSSON, E. G. Reconfigurable intelligent surfaces: Three myths and two critical questions. *IEEE Communications Magazine*, 2020, vol. 58, no. 12, p. 90–96. DOI: 10.1109/MCOM.001.2000407

[17] BJÖRNSON, E., WYMEERSCH, H., MATTHIESEN, B., et al. Reconfigurable intelligent surfaces: A signal processing perspective with wireless applications. *IEEE Signal Processing Magazine*, 2022, vol. 39, no. 2, p. 135–158. DOI: 10.1109/MSP.2021.3130549

[18] BJÖRNSON, E., SANGUINETTI, L. Power scaling laws and near-field behaviors of Massive MIMO and intelligent reflecting surfaces. *IEEE Open Journal of the Communications Society*, 2020, vol. 1, p. 1306–1324. DOI: 10.1109/OJCOMS.2020.3020925

[19] WU, Q., ZHANG, R. Towards smart and reconfigurable environment: Intelligent reflecting surface aided wireless network. *IEEE Communications Magazine*, 2020, vol. 58, no. 1, p. 106–112. DOI: 10.1109/MCOM.001.1900107

[20] HAROON AURANGZEB, M., AKRAM, F., RASHID, I., et al. Sparse RIS in multi user MIMO wireless system. In *16th International Conference on Open Source Systems and Technologies (ICOSST)*. Lahore (Pakistan), 2022, p. 1–5. DOI: 10.1109/ICOSST57195.2022.10016816

[21] MARINOVIC, I., ZANCHI, I., BLAZEVIC, Z. Estimation of channel parameters for "Saleh-Valenzuela" model simulation. In *18th International Conference on Applied Electromagnetics and Communications (ICECOM)*. Dubrovnik (Croatia), 2005, p. 1–4. DOI: 10.1109/ICECOM.2005.204926

[22] WEI, X., SHEN, D., DAI, L. Channel estimation for RIS assisted wireless communications - Part I: Fundamentals, solutions, and future opportunities. *IEEE Communications Letters*, 2021, vol. 25, no. 5, p. 1398–1402. DOI: 10.1109/LCOMM.2021.3052822

[23] DONOHO, D. L. Compressed sensing. *IEEE Transactions on Information Theory*, 2006, vol. 52, no. 4, p. 1289–1306. DOI: 10.1109/TIT.2006.871582

[24] BARANIUK, R. G. Compressive sensing. *IEEE Signal Processing Magazine*, 2007, vol. 24, no. 4, p. 118–120. DOI: 10.1109/MSP.2007.4286571

[25] DUARTE, M. F., ELDAR, Y. C. Structured compressed sensing: From theory to applications. *IEEE Transactions on Signal Processing*, 2011, vol. 59, no. 9, p. 4053–4085. DOI: 10.1109/TSP.2011.2161982

[26] CANDES, E. J., WAKIN, M. B. An introduction to compressive sampling. *IEEE Signal Processing Magazine*, 2008, vol. 25, no. 2, p. 21–30. DOI: 10.1109/MSP.2007.914731

[27] AKRAM, F., RASHID, I., GHAFOOR, A., et al. Fast convergence algorithms for coherence optimization of Rank-1 Grassmannian codebooks. *Radioengineering*, 2019, vol. 28, no. 2, p. 457–463. DOI: 10.13164/re.2019.0456

About the Authors ...

Muhammad HAROON AURANGZEB received his bachelor's degree in Telecommunication Engineering from the National University of Science and Technology (NUST), Pakistan, in 2002, and master's degree in Communication Technology from NUST in 2013. He is currently Ph.D. student from NUST, Pakistan. Wireless communication, compressed sensing, and mm-wave hybrid MIMO systems are among his research interests.

Faisal AKRAM graduated with a bachelor's degree in Telecommunication Engineering from the National University of Science and Technology (NUST), Pakistan, in 2005. Later earned a master's degree in Communication Technology from University of Ulm, Germany and a Ph.D. from NUST Pakistan. Wireless communication, compressed sensing, mm-wave hybrid MIMO systems, and channel coding are some of his areas of interest in study.

Imran RASHID earned his B.E. in Electrical (Telecommunication) Engineering from NUST in Pakistan and M.S in Telecommunication Engineering (Optical Communication) from D.T.U. Denmark, completed his Ph.D. in Mobile Communication from the University of Manchester in the United Kingdom. His areas of interest include wireless and mobile technology, networks and cyber security, compressed sensing for MIMO OFDM systems

Attiq AHMED graduated with a Ph.D. in Electrical Engineering in 2016 from Pakistan's National University of Sciences and Technology (NUST). He is an Assistant Professor at NUST. Image/Signal processing, MIMO system is one of his research areas.